



Adsorption studies of Eu(III) ions from aqueous solutions by a synthesized copper magnetic ferrite nanoparticles as low-cost adsorbent

M. R. Hassan^{1,*}  and M. I. Aly²

¹Nuclear Research Center, Egyptian Atomic Energy Authority, P.O. 13759, Inshas, Cairo, Egypt

²Hot Laboratories and Waste Management Center, Egyptian Atomic Energy Authority, P.O. 13759, Inshas, Cairo, Egypt

Received: 13 April 2021

Accepted: 18 June 2021

Published online:

1 July 2021

© The Author(s), under exclusive licence to Springer Science+Business Media, LLC, part of Springer Nature 2021

ABSTRACT

In this work, the synthesis of CuFe_2O_4 magnetic nanoparticles was carried using gelatin as a novel technique and tested for Eu(III) adsorption from aqueous solutions. The synthesized magnetic nanoparticles were characterized using different spectroscopic tools such as TEM, XRD, and FTIR. The parameters affecting the Eu(III) adsorption were also discussed. The batch technique results indicated that Eu(III) recovery from an aqueous solution onto CuFe_2O_4 magnetic nanoparticles increased with the increasing pH. It reached a maximum Eu(III) adsorption value at pH 5. The kinetic study indicated that the adsorption of Eu(III) process was fitted well to the pseudo-second-order kinetic model. In contrast, the isotherm study revealed that the Eu(III) adsorption process obeyed the Langmuir isotherm model. The calculated maximum adsorption capacity, q_{max} , was found to be ≈ 60.82 mg/g. Thermodynamic parameters were computed, which suggested that the reaction is spontaneous. The regeneration test reveals that CuFe_2O_4 nanoparticles with 0.1 M HNO_3 could desorb Eu(III) and that the high adsorption potential for five regeneration cycles can be maintained. The applicability of CuFe_2O_4 nanoparticles for removing Eu(III) and Cs(I) from simulated wastewater was attained with percent removal of 98.3 and 86%, respectively.

1 Introduction

The preconcentration of radionuclides coming from liquid effluents of some industries and laborites to the aquatic system causes toxicity problems to the living organisms in the environment. The accumulations of such radionuclides in the aquatic system may

also be harmful to human causing health hazards. The release of such toxic pollutants in the aquatic system may be decreased by different recovery methods [1, 2].

Due to its importance europium has various uses and technological applications. Europium is used in printing notes in euro banknotes due to its red glow

Address correspondence to E-mail: muhmmmed_refait@yahoo.com

under ultraviolet. Europium has low-energy lights that provide more natural light, and europium is used to manufacture control rods used in nuclear reactors due to its higher neutron-absorbing property. The higher consumption of europium in the industry could increase its release in the living ecosystem [3].

Among different chemical separation techniques examined for dynamic removal of europium from industrial effluents such as precipitation, membrane filtration, and adsorption technique, it was found that the adsorption technique is more effective due to its low-cost little by-product in addition to the ease of operation [4].

Different adsorptive materials were used for the adsorption of the trivalent lanthanides/actinides, such as carbon charcoal [5, 6], iron oxide [7–9], and clay minerals [10, 11].

Due to their great surface area, besides high adsorption capacities, it was found that nanomaterials played an important role in the environmental remediation, including the removal of aqueous pollutants, the adsorption of europium from aqueous solutions was provided by [12, 13]. The limitation of such adsorption materials on the practical scale is the difficulty of their separation from aqueous solutions whereas; NMPs nonmagnetic particles can be easily separated from such solutions by applying an external magnetic field giving good separation with high-adsorption capacities [14, 15].

In this concern, this work aims to prepare magnetic nanoparticles, namely CuFe_2O_4 nanoparticles, using a sol–gel method. The characterization of the synthesized nano-adsorbent was done by means of available spectroscopic tools such as SEM, scanning electron microscope in addition to (FT-IR) Fourier transform infrared and (XRD) X-ray diffraction and (TEM) to determine the exact surface morphology and the predicated structure, respectively. The prepared Nano-adsorbent was tested for the adsorption of Eu(III) ions from an aqueous medium. The various parameters affecting Eu(III) adsorption using CuFe_2O_4 Nano adsorbent, such as pH, contact time, initial metal concentration, and temperature, were also provided.

2 Experimental

2.1 Preparation of adsorbent

The synthesis of magnetic ferrites nano-adsorbent was carried out using a sol–gel method through gelatin. Equimolar amounts of the copper nitrate and iron nitrate were mixing in 100 mL solution using deionized water. The gelatin solution was prepared by dissolving 10 g of gelatin in deionized water with continuous stirring with gentle warm-up until a clear solution was provided. Then add the gelatin solution dropwise to the 100 mL nitrate solution of $\text{Cu}(\text{NO}_3)_2 \cdot 3\text{H}_2\text{O}$ and $\text{Fe}(\text{NO}_3)_3 \cdot 9\text{H}_2\text{O}$ with vigorous stirring at 80 °C a dry gel of magnetic CuFe_2O_4 ferrites was obtained. By adding the formed gel in a suitable crucible and the ignition at 500 °C for 2 h to remove the combined gelatin using a muffle furnace the magnetic CuFe_2O_4 ferrites nanoparticles were formed.

2.2 Materials

A standard stock solution of europium with a concentration of 1000 mg/L was obtained by dissolving appreciate weighting amount of europium oxide, Eu_2O_3 in the deionized water in 100 mL conical flask. Other working europium solutions of concentration varied from 10 to 100 mg/L were obtained by appreciates dilutions of the original stock solution.

The pH of the aqueous solution was measured and adjusted using a dilute concentration of sodium hydroxide and hydrochloric acid before mixing with the nano adsorbent using a water bath thermostatic shaker. All other chemicals used in this work are of analytical grade otherwise stated.

2.3 Analysis

In this work, an atomic absorption spectrometer of type (Thermo-electron (S4) model) was used in the estimation of the concentration of Eu(III) ions in the aqueous solutions. A pH meter (Hanna type) of the united glass electrode was used in the batch experiments to adjust the pH of the aqueous phase. The expected structure and the surface morphology of the prepared nano-adsorbent was confirmed using FT-IR of type (IR Prestige-21, Shimadzu, Japan) and (XRD) X-ray diffractometer, respectively.

2.4 Batch adsorption experiment

The sorption of Eu(III) ions by the CuFe_2O_4 nanoparticles was investigated in aqueous solutions at pH 5 and 25–55 °C. In general, 0.02 g CuFe_2O_4 (magnetic nano-adsorbent) was added to 15 mL of europium(III) solution. After agitation at 250 rpm by shaker, the magnetic nano-adsorbent was removed by a magnet from the solution. The solution pH was adjusted by 0.1 M HNO_3 or 0.1 M NaOH , and the Eu(III) ions were determined using Thermo-electron (S4) model, an atomic absorption spectrometer.

All measurements were repeated three times and average estimates were utilized in the graph. The sorption capacity q_e (mg/g) and percentage removal of Eu(III) from the solution (% Removal) were computed using Eqs. (1) and (2):

$$q_e = (C_0 - C_e) \frac{V}{M} \quad (1)$$

$$\% \text{Removal} = \frac{C_0 - C_e}{C_0} \times 100 \quad (2)$$

where, C_0 (mg/L) donates the initial Eu(III) concentration, whereas C_e (mg/L) refers to the concentration of Eu(III) in the solution at equilibrium. V (mL) is the volume of the solution, W (g) is the mass of CuFe_2O_4 . The investigational data were throughout the kinetic and isotherm theoretical models. The best-fit model demonstrates the most credible sorption mechanism.

To further confirm the correlation between theoretical data (derived from the isotherm and kinetic models) and experimental data, the non-linear regression Root Mean Square Error (RMSE), the Sum of Error Squares (SSE), and Chi-Squares (X^2) be calculated to estimate the degree to which a fitted isotherm and kinetic models matched with experimental data according to Eqs. (3), (4) and (5) [16]:

$$\text{RMSE} = \sqrt{\frac{1}{n-2} \sum_1^n (q_{e,\text{exp}} - q_{e,m})^2} \quad (3)$$

$$\text{SSE} = \frac{1}{n} \sum_{n=1}^{\infty} (q_{e,\text{exp}} - q_{e,m})^2 \quad (4)$$

$$X^2 = \sum_1^n \frac{(q_{e,\text{exp}} - q_{e,m})^2}{q_{e,m}} \quad (5)$$

where n represents the number of data points in each treatment period, $q_{e,\text{exp}}$ and $q_{e,m}$ are the experimental and calculated values of Eu(III) ions absorbed per unit mass of CuFe_2O_4 nanoparticles. The smaller

value of RMSE, SSE, and X^2 means the better fitting of the curve [17].

2.5 Desorption investigation

After the adsorption process, 3 g/L of loaded samples with Eu(III) were placed in contact with 0.01 M acid or base solutions as elution agents (H_2SO_4 , HCl , HNO_3 , NaOH) and shaken at 25 °C for 240 (min). A magnet was used to isolate the liquid phase from the solutions, which was then analyzed. In the regeneration process, the desorbing agent that achieved the highest percent of Eu(III) desorption from the loaded samples under investigation can be used. After the desorption process, CuFe_2O_4 nanoparticles was washed with deionized water several times and dried in an oven, then was used for the next adsorption–desorption cycle experiment. The desorption process was calculated using Eq. (6):

$$\text{Desorption } \% = \frac{\text{Amount of desorbed ions}}{\text{Amount of adsorbed ions}} \times 100 \quad (6)$$

3 Results and discussion

3.1 Characterization

The surface morphology of synthesized as-prepared CuFe_2O_4 nanostructures has been examined using SEM by a scanning electron microscope (SEM), and (Fig. 1a) shows a typical micrograph of the sample under low magnification. The product is predominantly nanorods with a diameter of ~10 nm. One can note the high tendency of the fine crystallites to form mini- or macro-agglomerates with irregular shapes and sizes. The agglomeration phenomenon was also viewed as small particles aggregated in order to achieve a lower free energy state [18].

Figure 1b shows the XRD micrographs of the synthesized nano-adsorbent, CuFe_2O_4 . The graph indicates that the presence of diffraction patterns peaks characterized for the formation of CuFe_2O_4 which is in agreement with (101, 112, 200, 202, 211, 220, 230, 400 and 422) JCPDS database. The estimated crystal size of CuFe_2O_4 was calculated using Scherrer's equation given by Eq. (7):

$$d = \frac{0.9\lambda}{\beta \cos\theta} \quad (7)$$

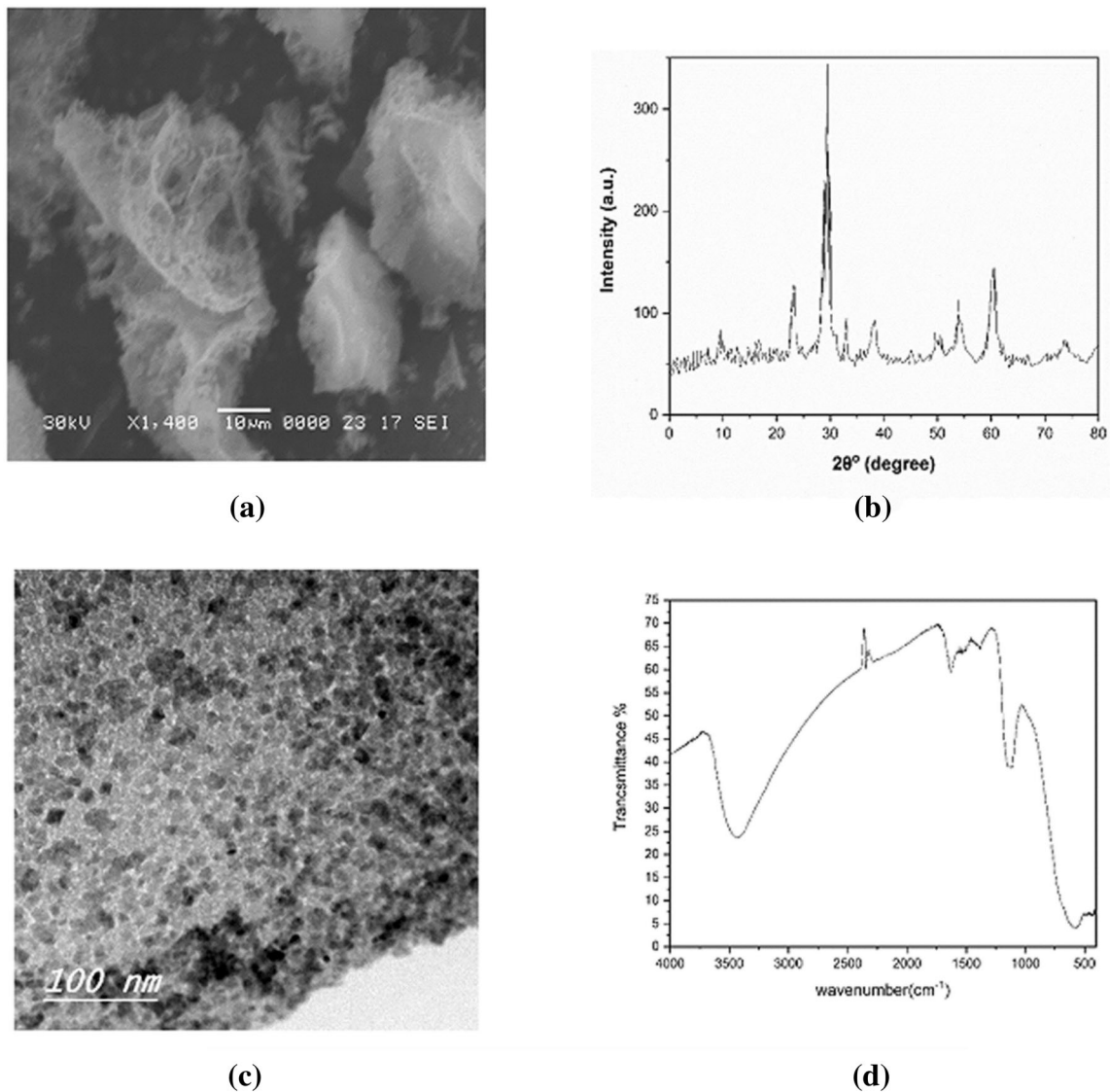


Fig. 1 **a** The SEM images, **b** XRD, **c** TEM and **d** FTIR of CuFe_2O_4

where, d donates the estimated crystal size, β refers to the full width at half maximum, whereas, λ expresses the wavelength of the incident X-ray, and θ is known as Bragg angle. It was found that the mean crystal size for as prepared CuFe_2O_4 nano-adsorbent to be about ≈ 10 nm [19].

Figure 1c gives TEM micrograph for the synthesized CuFe_2O_4 particles, it also shows the uniform shape of the powder with a good distribution of the particles. It was found that the estimated mean crystal size of CuFe_2O_4 particles from TEM micrograph was in the range of about ≈ 6 –12 nm which is in agreement with that obtained by XRD results and confirmed by SEM. From the results obtained of SEM,

TEM, and XRD, it was concluded that CuFe_2O_4 particles were prepared in a nano-size scale. Further characterizations were done using FT-IR spectrum in order to know the exact function groups that exist in the CuFe_2O_4 particles, (Fig. 1d) shows the FT-IR spectrum with two absorption bands at 400 cm^{-1} and 600 cm^{-1} that characterize to ferrites and metal ion oxygen vibration interactions in the octahedral and tetrahedral shapes [20]. In addition to the appearance of two absorption bands at 3200 cm^{-1} and 3600 cm^{-1} may be attributed to the presence (O–H) [21].

3.2 Batch adsorption studies

3.2.1 Effect of solution pH

The pH of the solution is an important parameter in the sorption process. The effect of pH on the removal of Eu(III) onto the prepared CuFe_2O_4 is showed in Fig. 2a. When the pH of the aqueous solution increased from pH 2 into pH 7 the removal percent of Eu(III) ions increased sharply from 20% up to 90%, respectively. While the further increase in pH, the removal percent increased slightly and attained the maximum value 99% at pH equals ~ 11 . Figure 2b shows that the predominant species below pH 6 are Eu^{3+} about 95%, whereas at pH ~ 7 it was found that 32% are Eu^{3+} and EuCO_3^{3+} in addition to other species $\sim 18\%$ $\text{Eu}(\text{OH})^{2+}$ and $\sim 10\%$ $\text{Eu}(\text{OH})^{2+}$ further increase of pH till ~ 8 the predominant ion species were found to be $\sim 58\%$ EuCO_3^{3+} and $\sim 20\%$

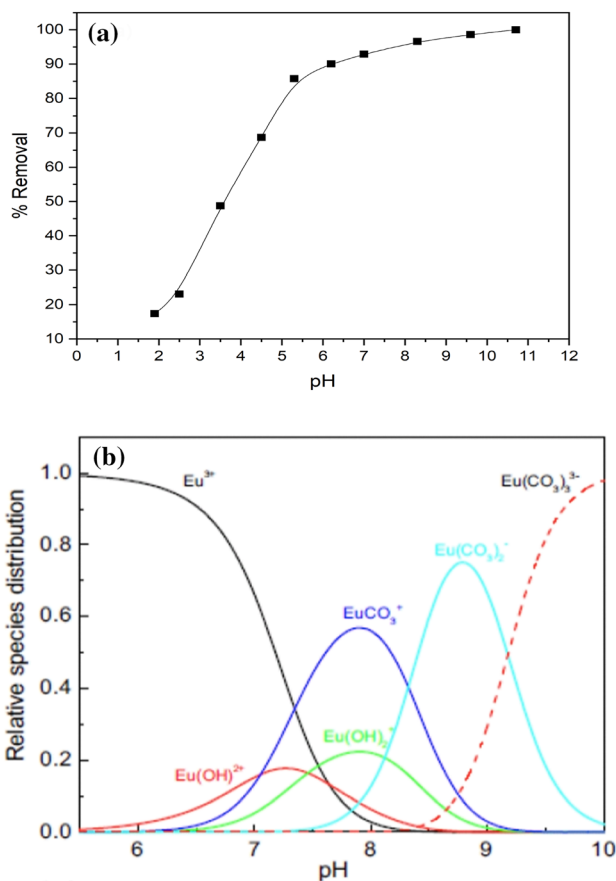


Fig. 2 **a** Effect of pH on the adsorption of Eu(III). Experimental conditions: [adsorbent dosage = 3 g/L; $(C_0) = 75$ mg/L; $(T) = 25$ °C]. **b** Relative species distribution of Eu(III) in 0.01 M NaClO_4 solution

$\text{Eu}(\text{OH})^{2+}$. With a further increase in the pH till ~ 9 and ~ 9.5 , the predominant species were found to be $\text{Eu}(\text{CO}_3)_2^{2-}$ and $\text{Eu}(\text{CO}_3)_3^{3-}$, respectively [22].

Therefore, the high values of the removal percent with the increase in pH could be explained by a low pH. There are electrostatic interactions between hydrogen ions and metal ions, and these effects are diminished at higher pH values [23].

3.2.2 Effect of adsorbent dosage

Figure 3 shows the effect of CuFe_2O_4 nanoparticles dosage (0.5–3.5 g/L) on removing Eu(III) ions. As can be seen from Fig. 3, when the initial concentration of the Eu(III) ions solution is 75 mg/L and volume is 15 mL, with the increase of the dosage of CuFe_2O_4 nanoparticles from 0.75 to 3 g/L, the removal percent (% R) of Eu(III) ions using CuFe_2O_4 nanoparticles increased to 85.7% and the uptake (q_e) decreased. The removal percent (% R) Eu(III) ions increased to 100% with an increase in CuFe_2O_4 nanoparticles dosage from 3 to 5.25 g/L, and the uptake (q_e) decreased more. The rise in Eu(III) ions with increasing dosage of CuFe_2O_4 nanoparticles can be attributed to the increase in the adsorption sites available on the surface of the CuFe_2O_4 nanoparticles [24, 25].

3.2.3 Effect of contact time

The effect of the contact time on the sorption of europium ions from the aqueous solution was investigated in the time range (5–240 min) (Fig. 4). From the results of contact time, it was concluded that the adsorption capacity, q_e of europium ions

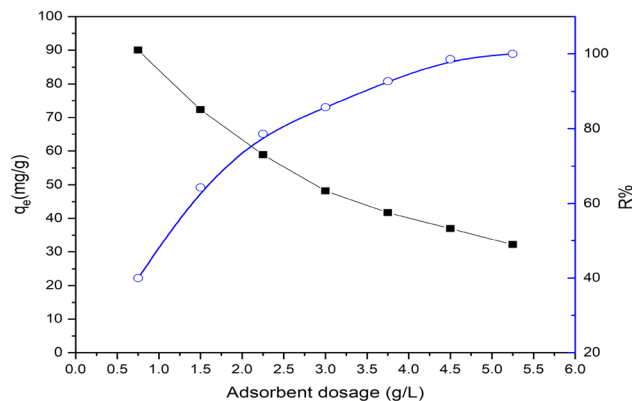


Fig. 3 Effect of CuFe_2O_4 nanoparticles dosage on Eu(III) ions adsorption. Experimental conditions: [adsorbent dosage = 0.75–5.25 g/L; pH 5; $(C_0) = 75$ mg/L; $(T) = 25$ °C]

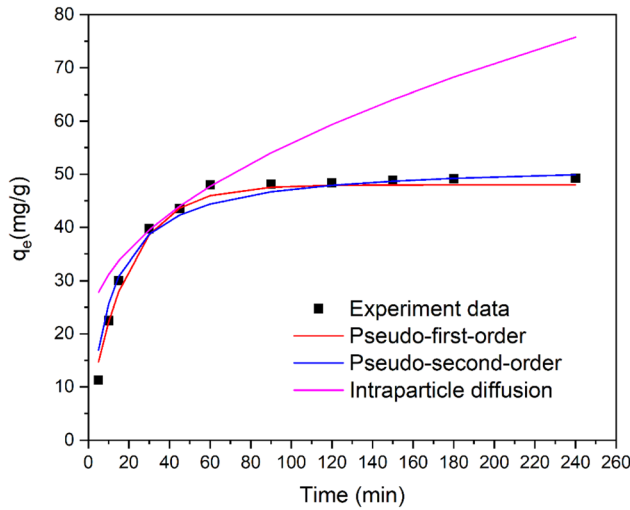


Fig. 4 Effect of contact time on adsorption of Eu(III). Experimental conditions: [pH 5; adsorbent dosage = 3 g/L; (C₀) = 75 mg/L; (T) = 25 °C]

increased from 10 mg/g up to 45 mg/g with the increase in contact time from 5 to 60 min, while the further increase in the contact time there no effect the capacity of adsorption. The equilibrium was reached at 60 min. The higher adsorption capacity at lower contact time may be interpreted by the availability of non-occupied adsorption sites, which decreases with further contact by forming a monolayer on the adsorbent surface [25].

3.2.3.1 Kinetic investigations The experimental data were analyzed using the well-known kinetic models such as intraparticle diffusion and pseudo first order and pseudo second order kinetic models to interpret the removal of europium ions by the synthesized CuFe₂O₄ adsorbent beside the rate-determining step of the adsorption process. Consider full surface coverage of the adsorbent with the europium ions, and under the ideal conditions, the pseudo first order kinetic model could be given using Eq. (8): [26];

$$\log(q_e - q_t) = \log q_e - K_1 \left(\frac{t}{2.303} \right) \tag{8}$$

where, q_e (mg/g) and q_t (mg/g) represent the quantity of Eu(III) ions transferred to the CuFe₂O₄ surface at the equilibrium and at any time, t (min), respectively. K_1 (L/min) refers to the energy of the adsorption rate constant.

The relation between the $\log(q_e - q_t)$ and the time (t) is represented in (Fig. 5a), and from the slope and the intercept of the straight lines, the values of K_1 and

q_e were calculated. Comparing the experimental and theoretical values of the adsorption capacity q_e (mg/g) in addition to the value of correlation coefficient, R^2 , it was concluded that the adsorption of europium ions by the synthesized CuFe₂O₄ is not fitted to the pseudo first-order kinetic model (Table 1). The pseudo-second order kinetic model [27] could be expressed using Eq. (9):

$$\frac{t}{q_t} = \frac{1}{K_2 q_e^2} + \frac{t}{q_e} \tag{9}$$

where, q_e (mg/g) and q_t (mg/g) represent the adsorbed Eu(III) ions amounts at the equilibrium and at any time, t (min), respectively. K_2 (g/mg/min) refers to second order rate constant. The relation between the t/q_t and the time (t) is represented in (Fig. 5b), and from the slope and the intercept of the straight lines, the values of K_2 and q_e were calculated. The experimental value of q_e (48 mg/g) is in agreement with the obtained theoretical value of q_e (50 mg/g) beside the value of R^2 (0.998). It was concluded that the adsorption of europium ions obeys the second order kinetics model [28] (Table 1).

Further information about the mechanism of the adsorption of europium ions by MNPs, CuFe₂O₄. The intra-particle diffusion should be applied to the experimental data was given by weber and Morris 1963 [29, 30], the intra-particle diffusion is provided by Eq. (10):

$$q_t = K_{diff} t^{0.5} + C \tag{10}$$

where, K_{diff} (mg/g min^{1/2}) donates the rate constant of the intra-particle diffusion, C refers to the intercept, which represents the mass transfer residence belongs to the boundary layer thickness. The greater the value of the intercept C means that the surface coverage becomes more thickness and participating in the rate-determining step [31, 32].

Plotting of q_e and $t^{0.5}$ in (Fig. 5c) and the intercept and the slope of the linear part give the value of C and K_{diff} , respectively (Table 1). The beginning part of the nonlinear curve represents the sorption boundary effect, while the second part provides the slow adsorption step or rate-controlling step. Whereas the plateau represents the equilibrium that occurred at the surface boundary, the intraparticle diffusion not the only rate step determining the mechanism of the adsorption of europium ions by CuFe₂O₄ nano-particles [33, 34].

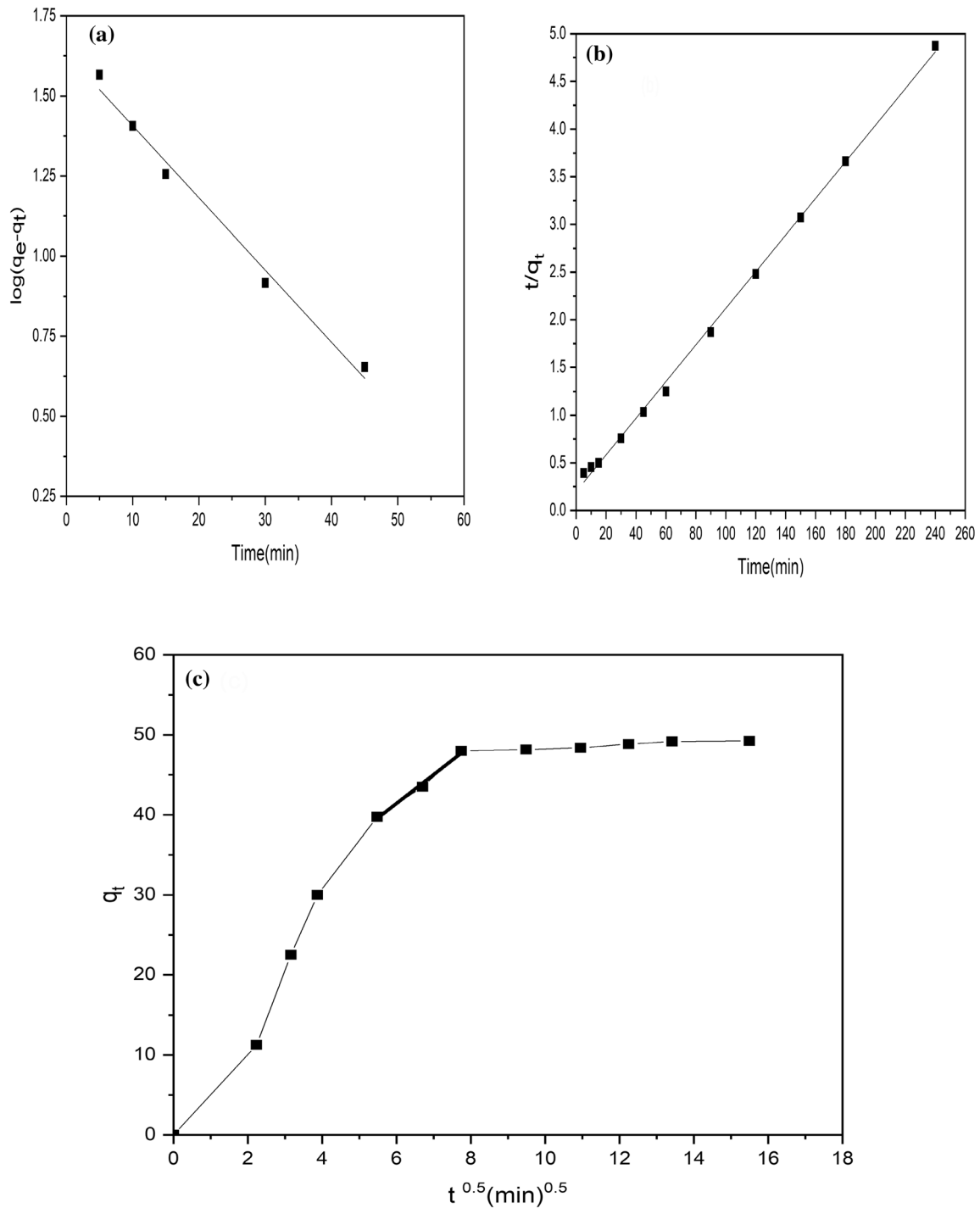


Fig. 5 **a** Pseudo-first-order, **b** Pseudo-second-order and **c** intra-particle diffusion plot for sorption kinetics of europium(III)

3.2.4 Effect of initial europium(III) ion concentration

The Influence of initial Eu(III) concentration on its sorption from the aqueous solution by CuFe₂O₄ was investigated in the concentration range 50–200 mg/L (Fig. 6). It was noticed that the sorption capacity of

Eu(III) increased from 30 mg/L into 55 mg/L when the initial Eu(III) concentration, C_o increased from 50 to 120 mg/L, respectively. It was noticed that no change in adsorption capacity increased in the concentration of Eu(III) up to 200 mg/L, i.e., the saturation of active sorption sites. It is concluded that the

Table 1 Kinetic constants for adsorption of europium(III) onto CuFe₂O₄

Model	Parameter	Value
Pseudo-first-order model	$q_{e,exp}$ (mg/g)	48
	K_1 (1/min)	0.05
	$q_{e,com}$ (mg/g)	42.85
	R^2	0.984
	RMSE	1.704
	SSE	2.377
Pseudo-Second-order model	X^2	0.060
	K_2 (mg/mg min)	0.001864
	H_0 (mg/g min)	5.050505
	$q_{e,com}$ (mg/g)	50.056
	R^2	0.998
	RMSE	2.601
Intraparticle parameters	SSE	5.5382
	X^2	0.1380
	K_{diff} (mg/g min ^{1/2})	3.618
	C	19.711
	R^2	0.974
	RMSE	14.204
	SSE	165.07
	X^2	3.329

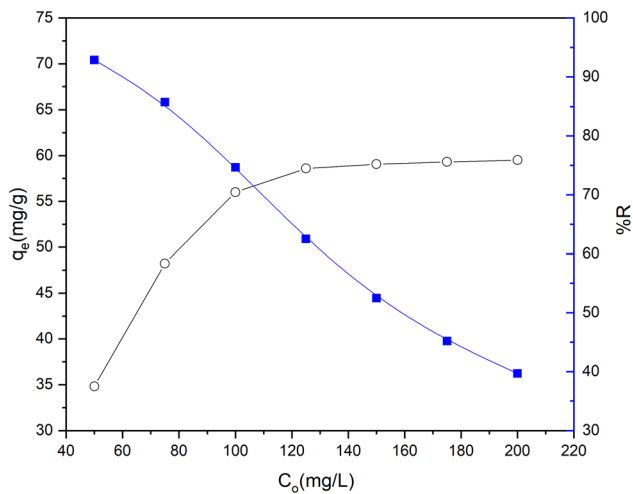


Fig. 6 Effect of initial concentration of europium(III). Experimental conditions: [adsorbent dosage = 3 g/L; pH 5; (C_0) = 50–200 mg/L; (T) = 25 °C]

sorption process depends on the initial Eu(III) concentration, and it chooses the [Eu(III)] = 75 mg/L throughout the rest of the batch experiments.

3.2.4.1 Isotherm study The analysis of the experimental data of europium ions adsorption by CuFe₂O₄

at equilibrium was described by commonly used two parameters isotherm models such as Langmuir, Freundlich, and Dubinin–Radushkevich; the nonlinear fitting of the tested models is shown Fig. 4 (Fig. 7a–c) at different temperatures 25 °C, 45 °C, and 65 °C, respectively.

Langmuir isotherm The Langmuir model provided the assumption of forming a homogeneous monolayer at the adsorbent surface [35]. The Langmuir model was applied to the adsorption equilibrium for CuFe₂O₄, using Eq. (11):

$$\frac{C_e}{q_e} = \frac{1}{bq_{max}} + \frac{C_e}{q_{max}} \tag{11}$$

where C_e (mg/L) refers to the concentration of Eu(III) ions at equilibrium, whereas the q_e (mg/g) is the amount of Eu(III) ions adsorbed by CuFe₂O₄ nanoparticles, b donates the Longmuir constant refers to the energy of adsorption of Eu(III) ions adsorbed by CuFe₂O₄ nanoparticles, and q_{max} is the maximum adsorption capacity (amount of adsorbate adsorbed per unit mass of the adsorbent to complete monolayer coverage (mg/g)). The plots of C_e/q_e against C_e give a linear relationship, and the values of the R^2 , Table 2 indicates that the adsorption of Eu(III) ions adsorbed by CuFe₂O₄ nanoparticles was fitted to the Langmuir isotherm model, Fig. 8a. The maximum adsorption capacity of CuFe₂O₄ nanoparticles for Eu(III) was 60.82 mg/g.

The Langmuir dimensionless equilibrium parameter R_L provides information about the affinity of the sorbate towards the adsorbent that was calculated using Eq. (12) [36]:

$$R_L = \frac{1}{1 + bC_0} \tag{12}$$

where b refers to the Langmuir constant and C_0 describes the maximum initial concentration of europium(III) ions. The values of R_L suggest the nature of the adsorption process; it was found that the value of R_L Table 2 less than 1 and more 0, indicating the adsorption of Eu(III) ions by CuFe₂O₄ is a favorable process [37].

Freundlich isotherm The linear form of the Freundlich isotherm model is given by relation (6). This model provides information about the interaction between the adsorbate and the adsorbent molecules in the case of heterogeneous surfaces. The model also describes the exponential decrease in the energy of

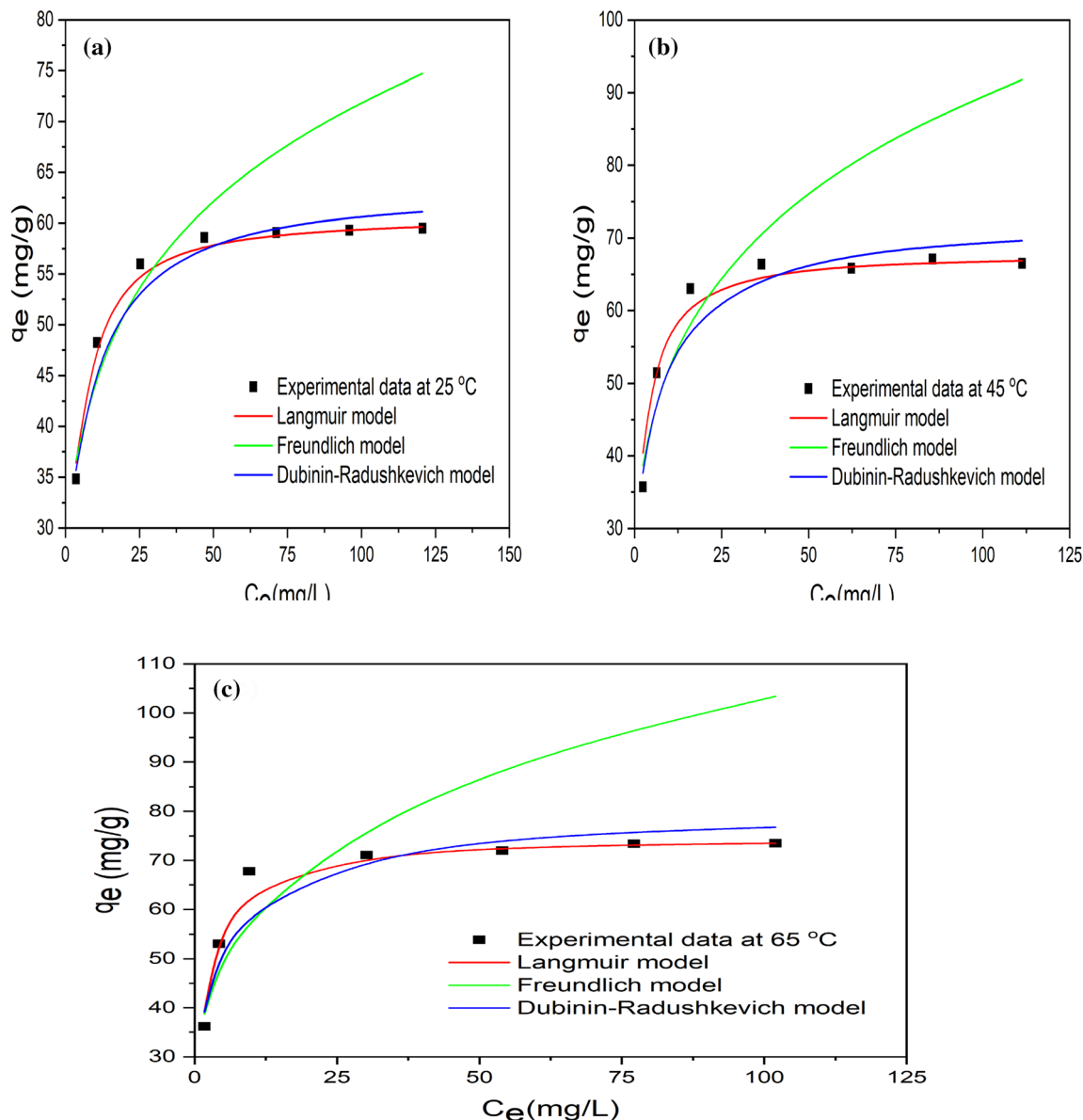


Fig. 7 a Sorption equilibrium isotherms for Eu(III) ions removal onto CuFe_2O_4 at temperature 25 °C, nonlinear fitting to Langmuir, Freundlich, and Dubinin–Radushkevich isotherm models. b Sorption equilibrium isotherms for Eu(III) ions removal onto CuFe_2O_4 at temperature 45 °C, nonlinear fitting to Langmuir,

Freundlich, and Dubinin–Radushkevich isotherm models. c Sorption equilibrium isotherms for Eu(III) ions removal onto CuFe_2O_4 at temperature 65 °C, nonlinear fitting to Langmuir, Freundlich, and Dubinin–Radushkevich isotherm models

adsorption with the number of possible active adsorption sites [38]. The Freundlich model is given by Eq. (13):

$$\log q_e = \log K_F + \frac{1}{n} \log C_e \quad (13)$$

where K_F refers to the Freundlich capacity and n donates the indicative constant of the intensity the adsorption intensity. (Fig. 8b) shows the linear relation fitting between $\log q_e$ against $\log C_e$. The relation

provides the applicability of the Freundlich model to this adsorbate–adsorbent system (Eu(III)– CuFe_2O_4 system). The n values were estimated by the slopes of the straight lines in (Fig. 8b) the n equals 4.93 provides that the CuFe_2O_4 is more efficient for the adsorption of europium ions from the aqueous solution based on the values of n , which lie between 1 and 10, so that this type of adsorption is a favorable process [39]. The Freundlich adsorption capacities, K_F

Table 2 Isotherm constants for adsorption of europium(III) onto CuFe₂O₄ at different temperatures

Isotherms models	Parameter	25 °C	45 °C	65 °C
Langmuir	q_{max} (mg/g)	60.82	67.94	74.62
	b (L/g)	0.417	0.619	0.642
	R_L	0.0228	0.0155	0.0150
	R^2	0.997	0.998	0.998
	RMSE	1.032	2.5949	2.2051
	SSE	0.7612	4.809	3.4733
	X^2	0.014	0.08003	0.0542
Freundlich	K_F (mg/g)	28.31	31.78	34.03
	n	4.93	4.44	4.16
	R^2	0.978	0.970	0.973
	RMSE	9.62	16.05	19.30
	SSE	66.18	184.19	266.18
	X^2	1.12	2.7062	3.64
	Dubinin-Radushkevich	q_m (mg/g)	0.4128	0.470
β (mol ² /kJ ²)		0.00646	0.00529	0.0044
E (kJ/mol)		8.7976	9.722	10.66
			0.944	0.920
R^2		0.978	0.944	0.920
RMSE		1.549	3.18	4.469
SSE		1.715	7.23	14.26
X^2		0.0319	0.1218	0.223

are estimated from the intercept of the straight lines of (Fig. 8b) and listed in Table 2.

Dubinin and Radushkevich isotherm To investigate the type of adsorption mechanism physical or chemical the data of adsorption should be analyzed by the Dubinin and Radushkevich isotherm model or the D–R model is given using Eq. (14):

$$\ln q_e = \ln q_m - \beta \varepsilon^2 \tag{14}$$

where q_e , (mg/g) is the amount of ions transferred to the adsorbent at equilibrium, q_m (mg/g) represents the maximum capacity. In contrast, β (mol²/kJ²) represents the energy of adsorption and ε refers to Polanyi potential that can be calculated using Eq. (15):

$$\varepsilon = RT \ln \left(1 + \frac{1}{C_e} \right) \tag{15}$$

where, R (8.314 kJ/mol/K) is the universal gas constant, T (K) represents the temperature in kelvin. C_e (mg/g) is the ion concentration at equilibrium. The following relation gives the free energy of adsorption, E , during the transfer of one mol of Eu(III) ions to the surface of the CuFe₂O₄ adsorbent and can be calculated using Eq. (16):

$$E = (2\beta)^{-1/2} \tag{16}$$

The illustrated data in (Fig. 8c) are fitted to the D–R isotherm model, and the values of E presented in (Table 2) suggesting that the adsorption of europium ions proceed via an ion-exchange mechanism with chemisorption process, since the value of E lies between 8 and 16 kJ/mol [16].

3.2.5 Effect of interfering ions

The effect of common interfering ions on Eu(III) adsorption onto CuFe₂O₄ nanoparticles was investigated. For this object, Eu(III) with the same interfering ions concentration was shaken under optimum conditions with 3 g/L CuFe₂O₄ nanoparticles. The amount of adsorbed Eu(III) ions was decided and presented in Table 3. It was observed that the uptake of Eu(III) was reduced by all cations that present in wastewater, such as Ca⁺, Na⁺, K⁺, and Mg²⁺. This is because cations may compete for sorption with metal ions [40].

The effect of interfering anions such as phosphate, carbonate, chloride, oxalate, nitrate, and sulfate was also studied. It was observed that all studied anions increased the uptake of Eu(III) except chloride. Thus,

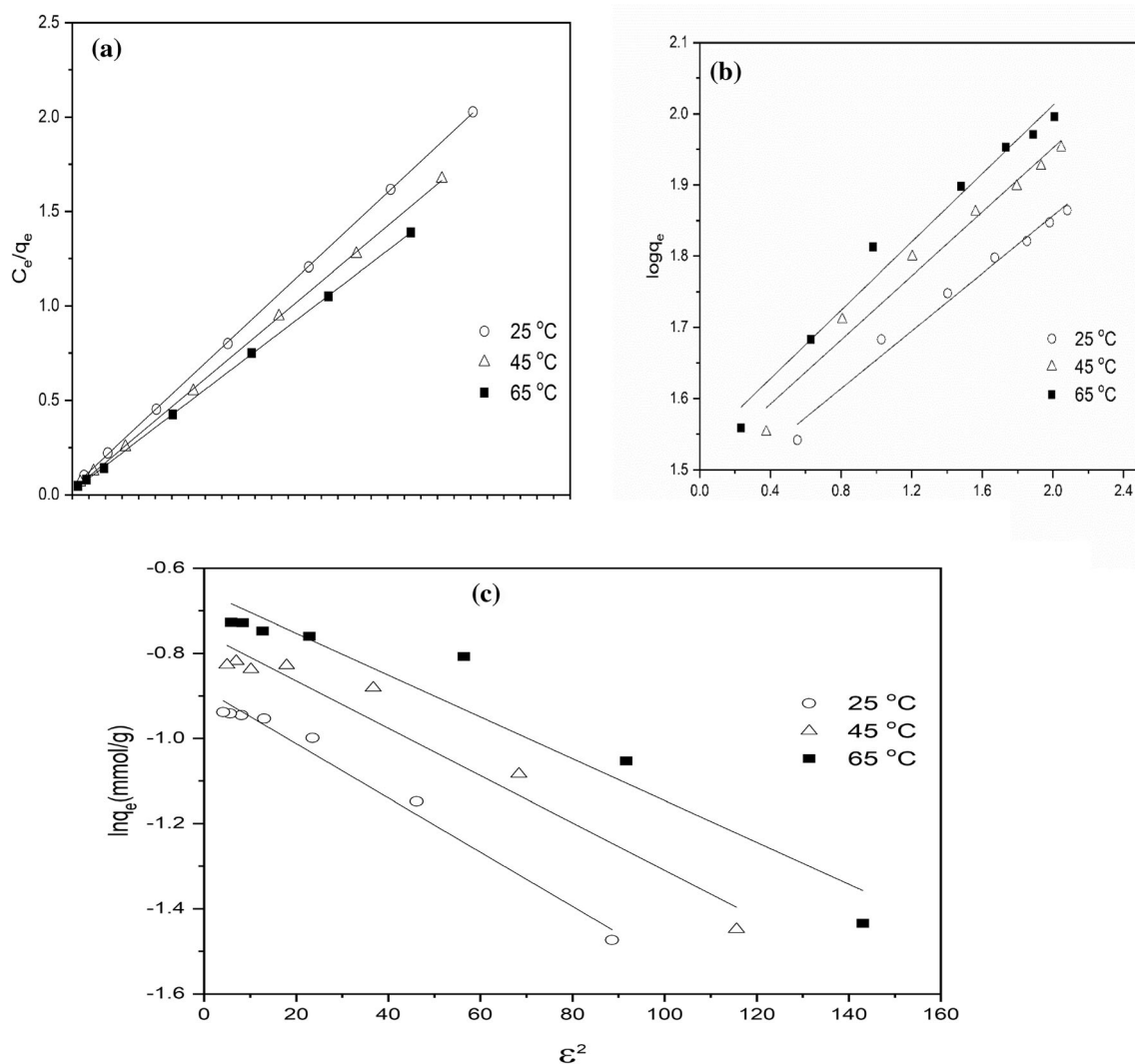


Fig. 8 **a** Langmuir plots, **b** Freundlich plots and **c** D–R plots for europium(III) adsorption

Table 3 Effect of common interfering ions on sorption of Eu(III) using CuFe_2O_4 nanoparticles

Cations	Uptake q_e (mg/g)	Anions	Uptake q_e (mg/g)
Pb^{2+}	60.82	PO_4^{3-}	79.5
Ca^{2+}	56	CO_3^{2-}	72.4
Na^+	56.3	$\text{C}_2\text{O}_4^{2-}$	70.2
K^+	58.5	Cl^-	55
Mg^{2+}	53.4	NO_3^-	61.3
–	–	SO_4^{2-}	62.8

some anions may form complexes with metal ions that influence the adsorption process.

3.2.6 Thermodynamic parameters

The effect of temperature on the adsorption capacity, q_e (mg/g) of europium ions the CuFe_2O_4 using nanoparticles with changing the initial metal concentration was investigated in the temperature range (25–65 °C). It was found by increasing the temperature from 25 to 65 °C, the adsorption capacity, q_e (mg/g) of europium ions increased from 60.82 to 74.62 mg/g (Fig. 9a). Thermodynamics parameters were estimated from the Vant Hoff equation that can be calculated using Eq. (17): [25]

$$\ln K_d = \frac{\Delta S^0}{R} - \frac{\Delta H^0}{RT} \quad (17)$$

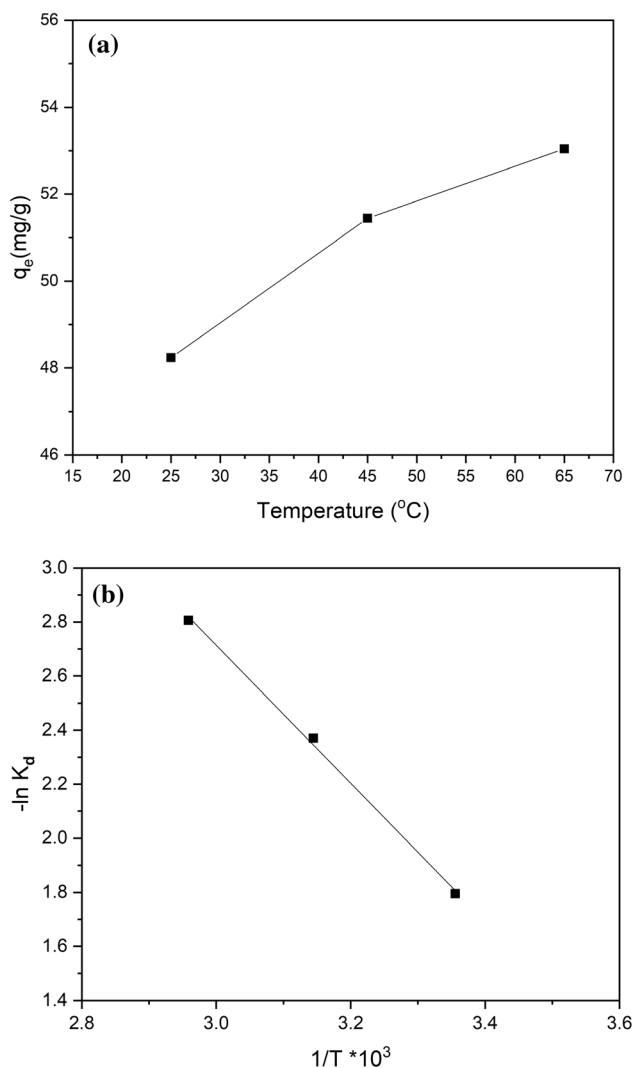


Fig. 9 **a** The effect of temperature on europium(III) uptake. Experimental conditions: [pH 5; adsorbent dosage = 3 g/L; (C₀) = 75 mg/L; (T) = 25–65 °C]. **b** Van't Hoff plots of europium(III) adsorption

where, *R* (8.314 J/mol K) donates the general gas constant, *T* (K°) refers to the absolute temperature; *K_d* (L/g) represents the distribution coefficient.

The standard enthalpy change (ΔH°) and the standard entropy change (ΔS°) are estimated using the slope and intercept of the plot of $\ln K_d$ versus ($1/T$) shown in (Fig. 9b), and the standard Gibbs free energy change (ΔG°) can be calculated using Eq. (18):

$$\Delta G^\circ = \Delta H^\circ - T\Delta S^\circ \tag{18}$$

The values of ΔH° (kJ/mol), ΔS° (J/mol/K), ΔG° (kJ/mol), and *K_d* are shown in Table 4. The negative sign of (ΔH°) provided that the adsorption of

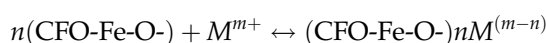
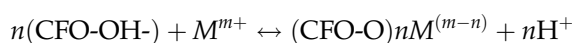
Table 4 Thermodynamic parameters of europium(III) adsorption onto CuFe₂O₄ at a different temperature

Temperature K	<i>K_d</i> L/g	ΔG° kJ/mol	ΔH° kJ/mol	ΔS° J/mol/K
298	0.1661	− 4.5004		
318	0.0934	− 6.3411	21.388	87.1981
338	0.0604	− 7.9802		

europium ions in this work is an endothermic process [41], and (ΔS°) has a positive sign indicating that the randomness of the investigated system. The negative sign of (ΔG°) indicated that the adsorption of europium ions is a spontaneous process and thermodynamically favorable [42].

3.3 Mechanism of CuFe₂O₄ nanoparticles adsorption

The adsorption process mechanism is a significant factor in understanding both the retention process and the material characteristics that enable the potential applications to design a new adsorbent. Electrostatic interaction is presented by ion exchange or Fe_{3- χ O₄} structures among the positively charged loaded on metal ions and the negative charged loaded on CuFe₂O₄ nanoparticles.



where CFO is the CuFe₂O₄ nanoparticles, *M^{m+}* represents the metal ions, and OH[−] and Fe-O[−] represent the anionic surface groups of CuFe₂O₄ nanoparticles.

The CuFe₂O₄ surface of nanoparticles is charged negatively when the number of protons decreases. Consequently, Eu(III) positive metal ion species is adsorbed by chemisorption or electrostatic attraction to the CuFe₂O₄ surface of nanoparticles [5].

3.4 Desorption and reusability studies

One of the main factors in applying adsorbents is their capacity for regeneration and reusability in another cycle. 0.01 M of nitric acid shows higher desorption efficiency than other elution agents. Therefore, nitric acid was chosen as a desorbing agent for CuFe₂O₄ nanoparticles then the different concentrations of nitric acid (0.01–0.1 M) were used

as elution agents. 0.1 M of nitric acid demonstrates the highest desorption efficiency with CuFe_2O_4 nanoparticles at approximately 87% (Table 5).

To determine the reusability of CuFe_2O_4 nanoparticles, Eu(III)'s adsorption capacity has been studied after regeneration (Fig. 10). The removal efficiency of Eu(III) is shown to be almost unchanged after the fifth regeneration.

3.5 Application study

A simulated wastewater solution containing europium ions was prepared by dissolving an appropriate amount of analytical grade chemical reagents in double-distilled water. The potential removal of Eu(III) from wastewater onto the synthesized MNPs, CuFe_2O_4 nanoparticles was achieved under optimized experimental conditions such as pH, mass, contact time [43]. The chemical composition of the prepared wastewater solution used in the application study is given in Table 6. The results obtained europium and cesium ions could be removed effectively from the simulated prepared wastewater, using the new synthesized MNPs CuFe_2O_4 nanoparticles with a percent removal of 98.3 and 86%, Eu(III) and Cs(I) ions, respectively. The application study concluded that the synthesized MNPs, CuFe_2O_4 nanoparticles consider an effective and potential adsorbent for the adsorption of europium ions from wastewater solution.

3.6 Comparative study

The efficiency of CuFe_2O_4 nanoparticles was compared to other adsorbents for Eu(III) adsorption. Table 7 shows the adsorption capacity values for many adsorbents. The CuFe_2O_4 nanoparticles were the third best adsorption capacity for Eu(III) among the seven indicated adsorbents, with a maximum adsorption capacity of 60.82 mg/g. These findings suggest that in addition to the low material costs, the removal capacity of Eu(III) is high, making it a viable

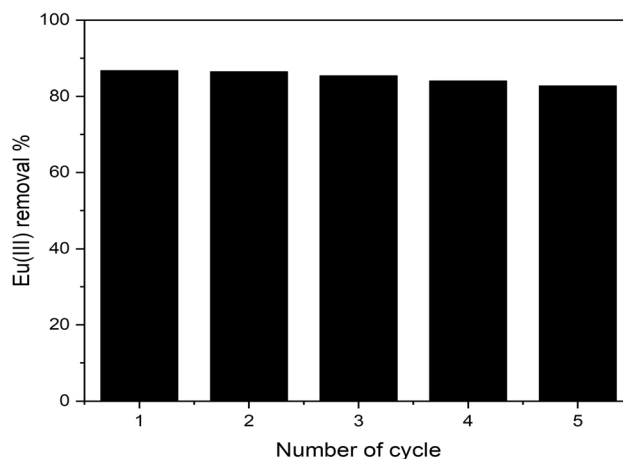


Fig. 10 Variation of Eu(III) removal efficiency onto CuFe_2O_4 nanoparticles as a function of regeneration cycle number. Desorption conditions: [0.1 M HNO_3 ; (T) = 25 °C]

and potential alternative because the majority of materials which have been produced and able to remove Eu(III) need more refined preparation techniques, thus raising operational costs.

4 Conclusion

The synthesis of magnetic CuFe_2O_4 nanoparticles was carried utilizing the sol–gel method. The characterization of the synthesized adsorbent was done by TEM, XRD, and FTIR proved that CuFe_2O_4 was prepared in a Nano size structure. The optimum conditions for the adsorption of Eu(III) by CuFe_2O_4 was found to be at a contact time of 60 min, the adsorbent weight of 3 g/L, and pH 5 at 25 ± 1 °C. The maximum adsorption capacity of europium from aqueous by CuFe_2O_4 is 60.82 mg/g. The isotherm investigation indicated that Eu(III)'s adsorption by CuFe_2O_4 proceeds via the chemisorption process. The kinetic study provided that Eu(III)'s adsorption by CuFe_2O_4 was fitted to the pseudo-second-order kinetic model and intraparticle diffusion. The thermodynamic investigations indicated that the adsorption of Eu(III)

Table 5 desorption of Eu(III) using different desorbing agents

No	The elution agents investigated, (0.01 M)	Desorption (%)	[HNO_3], M	Desorption, %
1	HNO_3	23.43	0.010	23.43
2	H_2SO_4	15.62	0.025	45.31
3	HCl	11.71	0.050	65.01
4	NaOH	4.68	0.100	87.1

Bold indicates the higher value of desorption percentage

Table 6 Chemical composition for simulated wastewater solution and removal outcomes achieved

Ions	Total hardness	Ca:Mg	SO ₄ ²⁻	Cl ⁻	NO ₃ ⁻	PO ₄ ³⁻	Oxalate	Cs(I)		Eu(III)	
								Added % removal	Added % removal	Added % removal	Added % removal
Conc (g/L)	0.003	1:1	0.03	0.02	0.06	0.001	0.001	0.005	86	0.03	98.3

Table 7 the maximum adsorption capacity of Eu(III) ions onto different adsorbents listed in the literature

Adsorbents	The max. adsorption capacity q_{max} (mg/g)	References
Graphene oxide nanosheet	175.4	[44]
ZSM-5	3.2	[45]
H-APC	46.5	[40]
HAPB9	74.42	[42]
Ion-imprinted nanofibers of PVDF/RTIL	22.37	[3]
Commercial titanium dioxide	5	[46]
Polycondensed perlite	20	[47]
CuFe ₂ O ₄ nanoparticles	60.82	This work

Bold indicates the high value of maximum adsorption capacity

by CuFe₂O₄ is an endothermic process. The effect of interfering ions was studied. It was observed that all studied anions increased the uptake of Eu(III) except chloride and all studied cations decreased the uptake of Eu(III). 0.1 M of nitric acid is an effective desorbing agent for Eu(III) desorption from CuFe₂O₄ nanoparticles and makes it ready for the next adsorption cycle. Europium and cesium ions removal from simulated wastewater solution was achieved with percent removal of Eu(III) and Cs(I) of 98.3 and 86%, respectively. Finally, the CuFe₂O₄ nanoparticles have shown to be a promising alternative adsorbent to adsorb and separate Eu(III) ions from wastewater.

Acknowledgements

Egyptian Atomic Energy Authority supported this work.

Declarations

Conflict of interest The authors declare that they have no conflict of interest.

References

1. P.D. Bhalara, D. Punetha, K. Balasubramanian, A review of potential remediation techniques for uranium(VI) ion retrieval from contaminated aqueous environment. *J. Environ. Chem. Eng.* **2**, 1621–1634 (2014)
2. S. Rao, J. Liang, W. Song, Accumulation of ¹⁵²⁺¹⁵⁴Eu(III) by *Aspergillus sydowii* and *Trichoderma harzianum*. *J. Environ. Radioact.* **193–194**, 75–81 (2018)
3. A. Rajhans, P.M. Gore, S.K. Siddique, B. Kandasubramanian, Ion-imprinted nanofibers of PVDF/1-butyl-3-methylimidazolium tetrafluoroborate for dynamic recovery of europium(III) ions from mimicked effluent. *J. Environ. Chem. Eng.* **7**, 103068 (2019)
4. D. Lin, M. Shi, Y. Zhang et al., 3D crateriform and honeycomb polymer capsule with nano re-entrant and screen mesh structures for the removal of multi-component cationic dyes from water. *Chem. Eng. J.* **375**, 121911 (2019)
5. M.M. Hamed, M.M.S. Ali, M. Holiel, Preparation of activated carbon from doum stone and its application on adsorption of ⁶⁰Co and ¹⁵²⁺¹⁵⁴Eu: equilibrium, kinetic and thermodynamic studies. *J. Environ. Radioact.* **164**, 113–124 (2016)
6. L. Xu, T. Zheng, S. Yang et al., Uptake mechanisms of Eu(III) on hydroxyapatite: a potential permeable reactive barrier backfill material for trapping trivalent minor actinides environ. *Sci. Technol.* **50**, 3852–3859 (2016)
7. C. Ding, W. Cheng, Y. Sun, X. Wang, Novel fungus-Fe₃O₄ bio-nanocomposites as high performance adsorbents for the removal of radionuclides. *J. Hazard. Mater.* **295**, 127–137 (2015)
8. A.C. Texier, Y. Andrès, C. Faur-Brasquet, P. Le Cloirec, Fixed-bed study for lanthanide (La, Eu, Yb) ions removal

- from aqueous solutions by immobilized *Pseudomonas aeruginosa*: experimental data and modelization. *Chemosphere* **47**, 333–342 (2002)
9. X. Wang, Y. Sun, A. Alsaedi, T. Hayat, X. Wang, Interaction mechanism of Eu(III) with MX-80 bentonite studied by batch, TRLFS and kinetic desorption techniques *Chem. Eng. J.* **264**, 570–576 (2015)
 10. Y. Sun, J. Li, X. Wang, The retention of uranium and europium onto sepiolite investigated by macroscopic, spectroscopic and modeling techniques *Geochim. Cosmochim. Acta* **140**, 621–643 (2014)
 11. Y. Zhu, H. Liu, T. Chen, B. Xu, P. Li, Kinetics and thermodynamics of Eu(III) adsorption onto synthetic monoclinic pyrrhotite. *J. Mol. Liq.* **218**, 565–570 (2016)
 12. R.S. Carvalho, A.L. Daniel-da-Silva, T. Trindade, Uptake of europium(III) from water using magnetite nanoparticles. *Part. Part. Syst. Charact.* **33**, 150–157 (2016)
 13. C.L. Chen, X.K. Wang, M. Nagatsu, Europium adsorption on multiwall carbon nanotube/iron oxide magnetic composite in the presence of polyacrylic acid environ. *Sci. Technol.* **43**, 2362–2367 (2009)
 14. M.I.A.A. Maksoud, A. El-ghandour, G.S. El-Sayyad et al., Tunable structures of copper substituted cobalt nanoferrites with prospective electrical and magnetic applications. *J. Mater. Sci.* **30**, 4908–4919 (2019)
 15. J.-M. Liu, Y.-H. Lu, Z.-F. Xu, R.-X. Wang, H.-C. Yan, X. Li, Effect of citric acid-to-nitrate ratio on combustion synthesis of CuFe_2O_4 for sodium-ion storage. *J. Mater. Sci.* **32**, 94–101 (2021)
 16. S.M. Yakout, M.R. Hassan, A.A. Abdeltawab, M.I. Aly, Sono-sorption efficiencies and equilibrium removal of triphenylmethane (crystal violet) dye from aqueous solution by activated charcoal. *J. Clean. Prod.* **234**, 124–131 (2019)
 17. M. Abbas, T. Aksil, M. Trari, Removal of toxic methyl green (MG) in aqueous solutions by apricot stone activated carbon-equilibrium and isotherms modeling. *Desalin. Water Treat.* **125**, 93–101 (2018)
 18. N. Rezlescu, E. Rezlescu, P.D. Popa, E. Popovici, C. Doroftei, M. Ignat, Preparation and characterization of spinel-type MeFe_2O_4 (Me = Cu, Cd, Ni and Zn) for catalyst applications. *Mater. Chem. Phys.* **137**, 922–927 (2013)
 19. F. Liu, T. Ren, C. Yang, L. Liu, A.Z. Wang, J. Yu, NiCuZn ferrite thin films for RF integrated inductors. *Mater. Lett.* **60**, 1403–1406 (2006)
 20. H. Harzali, F. Saida, A. Marzouki et al., Structural and magnetic properties of nano-sized NiCuZn ferrites synthesized by co-precipitation method with ultrasound irradiation. *J. Magn. Magn. Mater.* **419**, 50–56 (2016)
 21. P. Tang, J. Shen, Z. Hu et al., High-efficient scavenging of U(VI) by magnetic Fe_3O_4 @gelatin composite. *J. Mol. Liq.* **221**, 497–506 (2016)
 22. J.-Z. Xu, Q.-H. Fan, Z.-W. Niu, Y. Li, P. Li, W.-S. Wu, Studies of Eu(III) sorption on TiO_2 : effects of pH, humic acid and poly(acrylic acid). *Chem. Eng. J.* **179**, 186–192 (2012)
 23. S.I. Moussa, R.R. Sheha, E.A. Saad, N.A. Tadros, Synthesis and characterization of magnetic nano-material for removal of Eu^{3+} ions from aqueous solutions. *J. Radioanal. Nucl. Chem.* **295**, 929–935 (2013)
 24. L. Dong, C. Wu, Y. Han et al., Research on the application potential of spent biological activated carbon from BAC process to remove radionuclides Sr^{2+} from water. *J. Radioanal. Nucl. Chem.* **327**, 1179–1190 (2021)
 25. M.R. Hassan, M.I. Aly, Adsorptive removal of cesium ions from aqueous solutions using synthesized Prussian blue/magnetic cobalt ferrite nanoparticles. *Part. Sci. Technol.* **38**, 236–246 (2020)
 26. S. Lagergren, Zur theorie der sogenannten adsorption geloster stoffe. *Handlingar* **24**, 1–39 (1898)
 27. Y.S. Ho, G. McKay, Sorption of dye from aqueous solution by peat. *Chem. Eng. J.* **70**, 115–124 (1998)
 28. B.H. Hameed, Spent tea leaves: a new non-conventional and low-cost adsorbent for removal of basic dye from aqueous solutions. *J. Hazard. Mater.* **161**, 753–759 (2009)
 29. W. Weber, J. Morris, in *Proceedings of the second international conference on water pollution symposium* (Pergamon, Oxford, 1962), pp. 231–266
 30. B.H. Hameed, I.A.W. Tan, A.L. Ahmad, Adsorption isotherm, kinetic modeling and mechanism of 2,4,6-trichlorophenol on coconut husk-based activated carbon. *Chem. Eng. J.* **144**, 235–244 (2008)
 31. E. Demirbas, M.Z. Nas, Batch kinetic and equilibrium studies of adsorption of Reactive Blue 21 by fly ash and sepiolite. *Desalination* **243**, 8–21 (2009)
 32. D. Kavitha, C. Namasivayam, Experimental and kinetic studies on methylene blue adsorption by coir pith carbon. *Bioresour. Technol.* **98**, 14–21 (2007)
 33. A. Khaled, A. El Nemr, A. El-Sikaily, O. Abdelwahab, Treatment of artificial textile dye effluent containing Direct Yellow 12 by orange peel carbon. *Desalination* **238**, 210–232 (2009)
 34. S. Chen, J. Zhang, C. Zhang, Q. Yue, Y. Li, C. Li, Equilibrium and kinetic studies of methyl orange and methyl violet adsorption on activated carbon derived from *Phragmites australis*. *Desalination* **252**, 149–156 (2010)
 35. I. Langmuir, The adsorption of gases on plane surfaces of glass, mica and platinum. *J. Am. Chem. Soc.* **40**, 1361–1403 (1918)

36. A. Özer, D. Özer, A. Özer, The adsorption of copper(II) ions on to dehydrated wheat bran (DWB): determination of the equilibrium and thermodynamic parameters. *Process Biochem.* **39**, 2183–2191 (2004)
37. E. Malkoc, Ni(II) removal from aqueous solutions using cone biomass of *Thuja orientalis*. *J. Hazard. Mater.* **137**, 899–908 (2006)
38. H. Freundlich, W. Heller, The adsorption of cis- and trans-azobenzene. *J. Am. Chem. Soc.* **61**, 2228–2230 (1939)
39. G. McKay, H.S. Blair, J.R. Gardner, Adsorption of dyes on chitin. I. Equilibrium studies. *J. Appl. Polym. Sci.* **27**, 3043–3057 (1982)
40. H.M.H. Gad, N.S. Awwad, Factors affecting on the sorption/desorption of Eu(III) using activated. *Carbon Sep. Sci. Technol.* **42**, 3657–3680 (2007)
41. L. Dolatyari, M.R. Yaftian, S. Rostamnia, Adsorption characteristics of Eu(III) and Th(IV) ions onto modified mesoporous silica SBA-15 materials. *J. Taiwan Inst. Chem. Eng.* **60**, 174–184 (2016)
42. H.M.H. Gad, M.A. Youssef, Sorption behavior of Eu(III) from an aqueous solution onto modified hydroxyapatite: kinetics, modeling and thermodynamics. *Environ. Technol.* **39**, 2583–2596 (2018)
43. H.M.H. Gad, H.A. Omar, M. Aziz, M.R. Hassan, M. Khalil, Treatment of rice husk ash to improve adsorption capacity of cobalt from aqueous solution. *Asian J. Chem.* **28**, 385–394 (2016)
44. Y. Sun, Q. Wang, C. Chen, X. Tan, X. Wang, Interaction between Eu(III) and graphene oxide nanosheets investigated by batch and extended X-ray absorption fine structure spectroscopy and by modeling techniques. *Environ. Sci. Technol.* **46**, 6020–6027 (2012)
45. D.D. Shao, Q.H. Fan, J.X. Li et al., Removal of Eu(III) from aqueous solution using ZSM-5 zeolite. *Microporous Mesoporous Mater.* **123**, 1–9 (2009)
46. M. Bouby, J. Lützenkirchen, K. Dardenne et al., Sorption of Eu(III) onto titanium dioxide: measurements and modeling. *J. Colloid Interface Sci.* **350**, 551–561 (2010)
47. M.A. Youssef, M.R. El-Naggar, I.M. Ahmed, M.F. Attallah, Batch kinetics of ^{134}Cs and $^{152+154}\text{Eu}$ radionuclides onto poly-condensed feldspar and perlite based sorbents. *J. Hazard. Mater.* **403**, 123945 (2021)

Publisher's Note Springer Nature remains neutral with regard to jurisdictional claims in published maps and institutional affiliations.